Acta Astronautica 126 (2016) 395–410

Contents lists available at ScienceDirect

Acta Astronautica

journal homepage: www.elsevier.com/locate/aa

Effects of artificial gravity on the cardiovascular system: Computational approach

Ana Diaz Artiles [a,c,*,1], Thomas Heldt [b,2], Laurence R. Young [a]

[a] Department of Aeronautics & Astronautics, Massachusetts Institute of Technology, Cambridge, MA 02139, United States
[b] Institute for Medical Engineering & Science, Department of Electrical Engineering & Computer Science, Massachusetts Institute of Technology, Cambridge, MA 02139, United States
[c] Sibley School of Mechanical and Aerospace Engineering, Cornell University, NY 14850, United States

ARTICLE INFO

Article history:
Received 8 December 2015
Accepted 6 May 2016
Available online 9 May 2016

Keywords:
Mathematical model
Short-radius centrifuge
Ergometer exercise
Orthostatic intolerance
Human spaceflight countermeasure

ABSTRACT

Artificial gravity has been suggested as a multisystem countermeasure against the negative effects of weightlessness. However, many questions regarding the appropriate configuration are still unanswered, including optimal g-level, angular velocity, gravity gradient, and exercise protocol. Mathematical models can provide unique insight into these questions, particularly when experimental data is very expensive or difficult to obtain. In this research effort, a cardiovascular lumped-parameter model is developed to simulate the short-term transient hemodynamic response to artificial gravity exposure combined with ergometer exercise, using a bicycle mounted on a short-radius centrifuge. The model is thoroughly described and preliminary simulations are conducted to show the model capabilities and potential applications. The model consists of 21 compartments (including systemic circulation, pulmonary circulation, and a cardiac model), and it also includes the rapid cardiovascular control systems (arterial baroreflex and cardiopulmonary reflex). In addition, the pressure gradient resulting from short-radius centrifugation is captured in the model using hydrostatic pressure sources located at each compartment. The model also includes the cardiovascular effects resulting from exercise such as the muscle pump effect. An initial set of artificial gravity simulations were implemented using the Massachusetts Institute of Technology (MIT) Compact-Radius Centrifuge (CRC) configuration. Three centripetal acceleration (artificial gravity) levels were chosen: 1 g, 1.2 g, and 1.4 g, referenced to the subject's feet. Each simulation lasted 15.5 minutes and included a baseline period, the spin-up process, the ergometer exercise period (5 minutes of ergometer exercise at 30 W with a simulated pedal cadence of 60 RPM), and the spin-down process. Results showed that the cardiovascular model is able to predict the cardiovascular dynamics during gravity changes, as well as the expected steady-state cardiovascular behavior during sustained artificial gravity and exercise. Further validation of the model was performed using experimental data from the combined exercise and artificial gravity experiments conducted on the MIT CRC, and these results will be presented separately in future publications. This unique computational framework can be used to simulate a variety of centrifuge configuration and exercise intensities to improve understanding and inform decisions about future implementation of artificial gravity in space.

1. Introduction

The cardiovascular system experiences important changes during spaceflight in response to a weightlessness environment. These changes include the central fluid shift phenomenon, the reduction in total circulation blood volume, and a decrease in heart size, venous compliance, and baroreflex sensitivity [1–5]. In general, this adaptation is successful. However, the re-adaptation process when crewmembers return to a gravity environment is more problematic, and orthostatic intolerance may occur [6–8].

Several countermeasures are currently in place [1,9]. In general, they are system specific, focusing on one aspect of human deconditioning in space. In particular, cardiovascular countermeasures include aerobic exercise, fluid loading, the use of leg cuffs to reduce the amount of fluid shift from the lower extremities to the upper extremities, and the use of Lower Body

* Corresponding author at: Sibley School of Mechanical and Aerospace Engineering, Cornell University, NY 14850, United States.
E-mail addresses: ad877@cornell.edu, anadiaz@mit.edu (A. Diaz Artiles), thomas@mit.edu (T. Heldt), lry@mit.edu (L.R. Young).
[1] ORCID identifier: orcid.org/0000-0002-0459-9327.
[2] ORCID identifier: orcid.org/0000-0002-2446-1499.

http://dx.doi.org/10.1016/j.actaastro.2016.05.005
0094-5765/

Negative Pressure (LBNP) that induces a cardiovascular stress [1]. However, despite the variety of countermeasures, their effectiveness in terms of maintaining preflight levels has not been demonstrated, and their specificity and difficult application to several physiological systems at the same time makes their use difficult and time consuming [9–11]. Artificial gravity is seen as an integrated countermeasure capable of challenging several physiological systems at the same time [10]. In particular, short-radius centrifugation combined with exercise may be effective against cardiovascular deconditioning in space [12]. However, the centrifuge configuration still needs to be selected in order to maximize its effectiveness. These critical design questions include g-level, radius, gravity gradient, angular velocity, and exercise protocol [6,7].

Some of these questions can be resolved using ground analogs, like bed-rest [13–19]. However, others can be approached using mathematical simulations. An important advantage of computational modeling is that it allows the exploration of many different configurations with a large flexibility at a low computational cost. Guyton was the “pioneer’ of the quantitative physiological system analysis of circulation regulation. He developed a large circulatory model with hundreds of equations used to quantify the different subsystems of the circulation and their control [20]. His main contributions include (but are not limited to) the understanding of the interaction between venous return and cardiac function, the whole body autoregulation, renal body-fluid feedback mechanism in long-term blood pressure control, graphical analysis of physiological regulation, and quantitative computer modeling of physiological systems [21–23]. Although Guyton's work was focused on long-term steady-state cardiovascular responses, the principles he developed are still applicable, and are widely used in the field [24].

The cardiovascular system can be modeled using different approaches depending on the modeling objective and the assumptions on the spatial degrees of freedom. Three-dimensional (3D) models are used when detailed information about the blood flow in a particular region is needed. In these models, the fluid behavior is usually described by the Navier–Stokes equations for incompressible fluids. Despite the progress of current numerical methods, the computational cost of these models is very high, limiting their application to small localized regions. One-dimensional (1D) models assume axial symmetry and only have one degree of freedom, namely translation along the axial direction. These models are useful to analyze arterial wave propagation, and they are described by hyperbolic partial differential equations. Finally, zero-dimensional models (0D), or lumped-parameter models, represent the spatial variation in a highly aggregated manner, as they compartmentalize the cardiovascular system into discrete functional units. They describe the time evolution of the pressure and flow in each compartment using ordinary differential equations [25]. The objective of our modeling effort is to capture the beat-to-beat, short-term hemodynamic response to artificial gravity generated by a compact-radius centrifuge. Thus, a lumped-parameter model is the logical choice, since it provides beat-to-beat average variables (including pressures, flows, and volumes) at a low computational cost.

1.1. Modeling orthostatic stress

With regard to the cardiovascular adaptation to gravitational stress, many computational models have been developed with a large variety of temporal and spatial resolutions, depending on the representation and the objective of the model [25,26]. Various mathematical models investigate the physiological responses to postural changes, such as active standing [27], head-up tilt [28–31], or lower body negative pressure [28,32]. Some models were designed to explain observations seen during human spaceflight [31,33,34], including the recent Visual Impairment and elevated Intracranial Pressure (VIIP) syndrome [35].

For our purpose, the cardiovascular model to be developed needs to have enough compartments to capture the strong hydrostatic gradient generated by a compact-radius centrifuge. Heldt developed a lumped-parameter model using 21 compartments in order to simulate the short-term ($\approx$ 5 minutes), transient, beat-to beat hemodynamic response to gravitational stress, such as head-up tilt and lower body negative pressure [36]. The hemodynamic model included the systemic circulation (arterial system, microcirculation, and the venous system), the cardiac chambers, and the pulmonary circulation. The cardiovascular system was represented by seventeen vascular and four cardiac compartments grouped into four main sections: head and arms, thorax, abdomen, and legs. The full 21-compartment model is shown in Fig. 1 and is currently incorporated in the expanded research version of CVSim, a computational platform developed at the Harvard-MIT Division of Health Science and Technology [37]. Parameters such as compliance, volume, resistance, or vascular length (to determine the hydrostatic pressure) were estimated from the literature [36]. The model also incorporated the arterial baroreflex and the cardiopulmonary reflex to maintain blood pressure homeostasis during orthostatic stress. Based on the 21-compartment model developed by Heldt, Zamanian built a lumped-parameter hemodynamic model for the cardiovascular response to centrifugation [38]. This new model introduced the simulation of the hydrostatic pressure resulting from centrifugation as well as a model for the collapsibility of blood vessels under high orthostatic stress (negative transmural pressure). Simulations at 11.6 rpm, 22.9 rpm, and 29.4 rpm were validated with experimental measurements conducted in the Man Vehicle Laboratory using the MIT short-radius centrifuge.

Despite the broad range of applications, to our knowledge, no previous computational models have been applicable to exercise in altered gravity environments. In the current modeling effort, Heldt's and Zamanian's approaches are combined and upgraded with a new exercise module to develop a unique cardiovascular model capable of capturing the short-term, beat-to-beat hemodynamic responses to artificial gravity generated by a compact-radius centrifuge combined with lower-body ergometer (i.e. cycling) exercise. In the following sections, the mathematical details of the model are described so it can be reproduced by the reader. Additionally, a series of preliminary simulations are presented and discussed to show the model capabilities and potential applications.

2. Modeling approach

The cardiovascular system can be represented as a fluid vessel network with regulatory control systems. This fluid network can also be represented by electric circuit analogs [36,38,39]. Thus, the cardiovascular system can be represented by a series of vascular segments modeled by electric circuit blocks or compartments. The model developed by Heldt [36] and used in this work consists of fifteen compartments representing the systemic circulation, four compartments representing the cardiac chambers, and two compartments representing the pulmonary circulation. In addition, the model includes the two major reflex mechanisms concerning the short-term hemodynamic response to orthostatic stress, namely the arterial baroreflex and the cardiopulmonary reflex.

Centrifugation using a short-radius centrifuge induces a significant orthostatic stress in the cardiovascular system. The artificial gravity induces both a primary rapid fluid shift from the upper body to the lower extremities, and a secondary slower fluid shift from the intravascular to the interstitial fluid compartment.

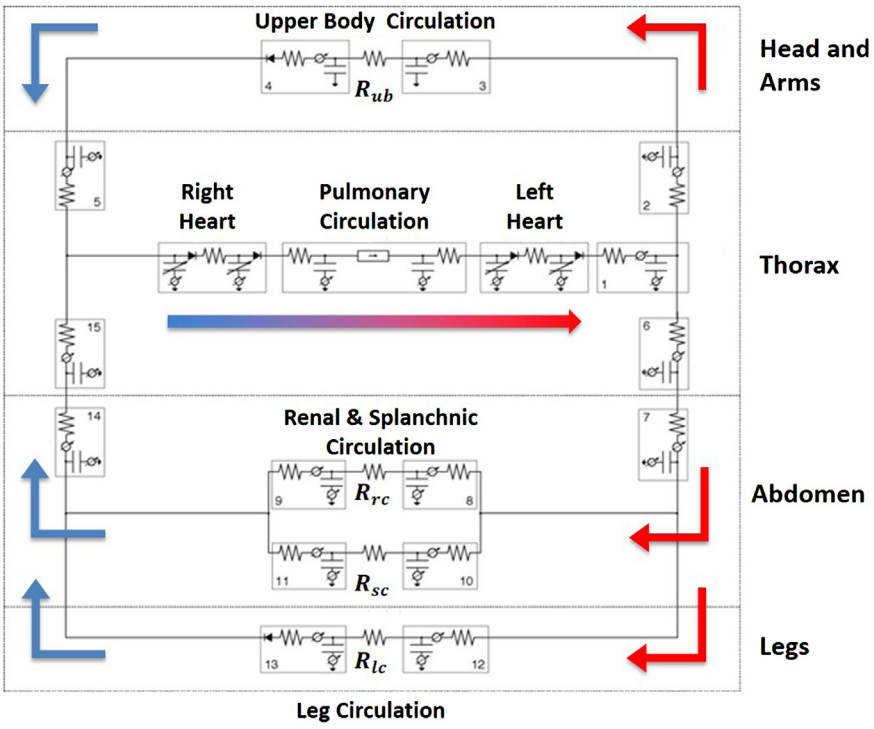

Fig. 1. Circuit representation of the 21-compartment cardiovascular model, composed of 4 sections: head and arms, thorax, abdomen, and legs. Four microvascular resistances are also included: upper body R_{ub}, kidneys R_{rc}, splanchnic R_{sc}, and legs R_{lc}. Figure modified from Heldt [36].

These shifts induce a cardiovascular state of central hypovolemia that triggers the regulatory mechanisms to counteract the reduction in blood pressure and central blood volume. These effects of centrifugation were modeled by Zamanian [38] and are incorporated in the model described here.

Lastly, exercise has a significant impact in the cardiovascular system. Exercise increases cardiac output and blood flow to the exercising muscles, located in the legs in the case of lower-body ergometer exercise. This effect is accompanied by a decrease in peripheral resistance in the working muscles to facilitate the attainment of the new and more demanding muscle metabolic needs. Other exercise effects are related to muscular contraction, such as the muscle-pump effect, which facilitates venous return, and the increase in intra-abdominal pressure. These effects, which were already considered by Heldt to some extent [36], are also incorporated in the model and they are further described in the following sections.

2.1. Systemic circulation

A single vascular segment is represented using the electric circuit analog show in Fig. 2. The compartment is characterized by an inflow resistance R_n, an outflow resistance R_{n+1}, and the pressure-volume relationship $V_n(P_n-P_e)$, or the capacity of the segment to store volume V_n given a transmural pressure $\Delta P = P_n-P_e$.

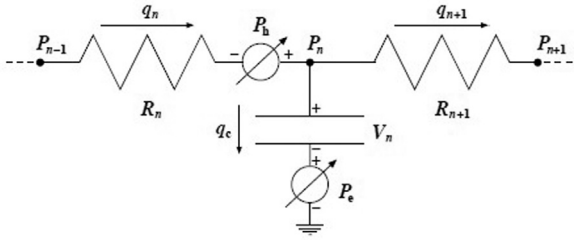

Fig. 2. Single compartment circuit representation [36].

In Fig. 2, P_{n-1}, P_n, P_{n+1} are the compartment pressures; P_h is the hydrostatic pressure; P_e is the external pressure (such as the intra-thoracic pressure, intra-abdominal pressure, or the muscle-pump pressure); q_n, q_{n+1}, q_c are the flow rates; V_n is the compartment volume; and R_n, R_{n+1} are the flow resistances. The flows are calculated using the following constitutive relations:

$$q_n = q_{n+1}+q_c$$

$$q_n = \frac{P_{n-1}-P_n+P_h}{R_n}$$

$$q_{n+1} = \frac{P_n-P_{n+1}}{R_{n+1}}$$

$$q_c = \frac{d}{dt}V_n = \frac{dV_n}{d(P_n-P_e)}\cdot\frac{d}{dt}(P_n-P_e) = \frac{dV_n}{d\Delta P_n}\cdot\frac{d\Delta P_n}{dt}$$

where $\frac{dV_n}{d\Delta P_n}$ is defined as incremental compliance C_n, that may be a function of transmural pressure.

In Heldt's model, the systemic circulation is represented by fifteen compartments, connected in series and parallel, representing three different functional units: the arterial system (aorta and arteries), the micro-circulation (arterioles and capillaries), and the venous system (venules, veins, and venae cavae). Thus, the entire model is described by a set of coupled first-order differential equations. The model architecture is shown in Fig. 1. The circulation is divided in four vascular beds. The upper body comprises the circulation of the head, the neck and upper extremities, and this accounts for 10% of total skeletal muscle mass, one third of the blood supply to the skin, and one half of the blood supply to the skeleton. The renal compartment represents the kidneys and the adrenal glands. The splanchnic compartment includes the gastrointestinal track, one third of the skin, and one half

of the adipose tissue. Lastly, the leg compartment comprises the lower extremities and the pelvic circulation. This accounts for 90% of the skeletal muscle, one half of the skeleton, one third of the skin, one half of the adipose tissue, and the pelvic organs [36].

Some parts of the systemic circulation show non-linear behaviors. For example, certain segments of the venous circulation only allow unidirectional flow due to the presence of unidirectional valves. Thus, unidirectional diodes are included in the compartments representing those regions, namely the venous upper body (compartment 4) and the venous leg circulation (compartment 13). The cardiac compartments also include unidirectional diodes representing the cardiac valves. Under certain conditions of orthostatic stress, pressure-volume relationships in some venous circulation regions can reach regimes where they show a non-linear behavior. Generally, blood vessels operate in the linear range (low transmural pressures), but at high transmural pressures, the compliance decreases and the vessel can reach the elastic limit. Therefore, the following non-linear relation between total volume, V_t, and transmural pressure, ΔP, is implemented in the compartments likely to be exposed to these non-linear regimes, namely the splanchnic (compartment 11), leg (compartment 13), and abdominal (compartment 14) venous compartments:

$$V_t = V_0 + \frac{2V_{max}}{\pi} \cdot arc\tan\left(\frac{\pi C_0}{2V_{max}} \cdot \Delta P\right) \quad \text{for} \quad \Delta P > 0$$

where V_{max} is the distending volume limit of the compartment, C_0 is the vascular compliance at zero transmural pressure, and V_0 is the venous unstressed volume or zero-pressure filling volume.

The numerical values assigned to all the physical parameters were estimated by Heldt based on the literature. In the model description, Heldt includes a very detailed discussion about the rationale of all these choices [36]. For each compartment, these parameters include values for resistance R, compliance C, zero-pressure filling volume V_0, and anatomical vertical length l_v (superior-to-inferior extension of the vascular segment). The leg anatomical vertical lengths l_{v12} and l_{v13} were adjusted to take into account the shorter configuration of the MIT centrifuge. In addition, the microvascular resistance values are also provided. Tables 1, 2, and 3 summarize the parameters of the systemic circulation.

2.2. Cardiac model

The four cardiac chambers are represented using time-varying elastance models proposed by Heldt [36]. Both the right heart (right atrium and right ventricle) and the left heart (left atrium and left ventricle) are modeled using the same circuit representation, shown in Fig. 3. The diodes represent the unidirectional nature of the blood flow in the cardiac chambers; R_{a-v} is the resistance due to the cardiac valves (tricuspid valve in the right heart, mitral valve in the left heart); P_a and P_v are the atrial and ventricular pressures; $C^a(t)$ and $C^v(t)$ are the atrial and ventricular capacitances; $E^a(t)$ and $E^v(t)$ are the atrial and ventricular elastances; and the time-varying pressure source P_{th} is the intrathoracic pressure.

Table 2
Parameter values assigned to the systemic microvascular resistances.

Parameter	Units	Microcirculation			
		Upper body R_{ub}	Kidneys R_{rc}	Splanchnic R_{sc}	Legs R_{lc}
R	PRU	3.3	4.1	2.4	3.9

Table 3
Parameter V_{max} (distending volume limit of the compartment) corresponding to the non-linear compartments.

Parameter	Units	Compartment index		
		11	13	14
V_{max}	ml	1500	1000	650

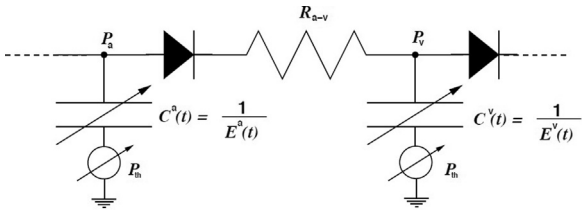

Fig. 3. Circuit representing the atrial and ventricular cardiac compartments. Figure taken from Heldt [36].

The normalized time-varying elastances for each one for the four cardiac chambers were taken to be identical, but each one scaled appropriately to account for the different end-systolic and end-diastolic compliances. Fig. 4 depicts the normalized time-varying elastance of the human left ventricle. The time-varying elastance in each one of the four chambers is modeled using the equation below, where the time interval of diastolic relaxation T_d^r is assumed to be one half of the systolic time interval T_s.

$$E(t) = \begin{cases} E_d + \frac{E_{es}-E_d}{2} \cdot \left\{1 - \cos\left(\pi \frac{t}{T_s}\right)\right\} & 0 \le t \le T_s \\ E_d + \frac{E_{es}-E_d}{2} \cdot \left\{1 + \cos\left(2\pi \frac{t}{T_s}\right)\right\} & T_s < t \le \frac{3}{2}T_s \\ E_d & \frac{3}{2}T_s < t \end{cases}$$

E_d and E_{es} are the diastolic elastance and end-systolic elastances respectively, and they take different values depending on the cardiac chamber. Table 4 summarizes the model parameters of the cardiac compartments.

The cardiac timing parameters include the atrial and ventricular systole duration, T_S^a and T_S^v, as well as the "P–R interval", i.e. the delay between the onset of the atrial and ventricular contraction T_{a-v}. Their values are assumed to be proportional to the square root of the R–R interval length (inter-beat interval) T_{RR} [36],

Table 1
Parameter values assigned to the systemic arterial compartments (1, 2, 3, 6, 7, 8, 10, and 12) and systemic venous compartments (4, 5, 9, 11, 13, 14, and 15). Parameters include compliance C, zero-pressure filling volume V_0, resistance R, and anatomical vertical length l_v (superior-to-inferior extension of the vascular segment).

Parameter	Units	Compartment index														
		1	2	3	4	5	6	7	8	9	10	11	12	13	14	15
C	$\frac{ml}{mmHg}$	0.28	0.13	0.42	7	1.3	0.21	0.10	0.21	5	0.42	50	0.42	27	1.3	0.5
V_0	ml	21	5	200	645	16	16	10	20	30	300	1146	200	716	79	33
R	PRU	0.007	0.003	0.014	0.11	0.028	0.011	0.010	0.010	0.11	0.07	0.07	0.09	0.10	0.019	0.008
l_v	cm	10.0	4.5	20.0	20.0	14.5	16.0	14.5	0.0	0.0	10.0	10.0	85.0	85.0	14.5	6.0

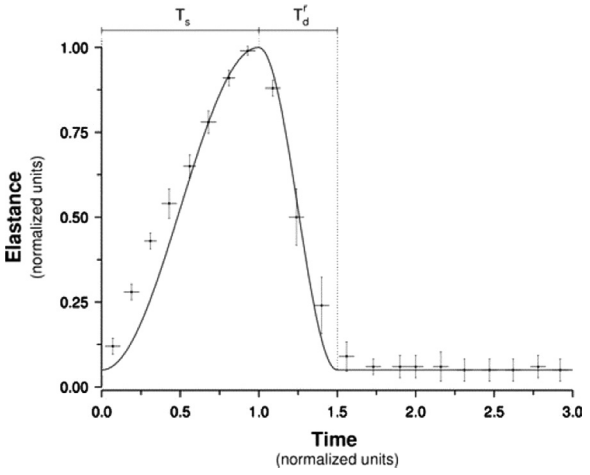

Fig. 4. Normalized time-varying elastance. T_s: systolic time interval; T_d^r: time interval of diastolic relaxation. Figure taken from Heldt [36].

Table 4
Cardiac parameters: E_d: diastolic elastance; E_{es}: end-systolic elastance; V_0: zero-pressure filling volume; R_{a-v}: resistance between atria and ventricles (right heart: tricuspid valve; left heart: mitral valve) Values taken from Heldt [36].

Parameter	Units	Right heart		Left heart	
		Atrium	Ventricle	Atrium	Ventricle
E_{es}	$\frac{\text{mm Hg}}{\text{ml}}$	0.74	1.3	0.61	2.5
E_d	$\frac{\text{mm Hg}}{\text{ml}}$	0.3	0.07	0.5	0.13
V_0	ml	14	46	24	55
R_{a-v}	PRU	0.006		0.010	

Table 5
Time parameters for the cardiac model: T_S^a: atrial systole duration; T_S^v: ventricular systole duration; T_{a-v}: delay between the onset of the atrial and ventricular contraction. T_{RR}: R–R interval length. Values taken from Heldt [36].

Parameter	Units	T_S^a	T_S^v	T_{a-v}
Time	s	$0.2\sqrt{T_{RR}}$	$0.3\sqrt{T_{RR}}$	$0.12\sqrt{T_{RR}}$

and they are summarized in Table 5.

The generation of heartbeats is represented using an Integral Pulse Frequency Modulation (IPFM) model [36,38,40]. The model represents the dynamics of the transmembrane potential $M(t)$, whose value at time t depends on the cumulative automaticity and the contribution of neural control (i.e. sympathetic or parasympathetic activity) since the last heartbeat or cardiac excitation time t_k-1.

$$M(t)=\int_{t_{k-1}}^{t} m(t)dt=\int_{t_{k-1}}^{t}\left(m_0+m_r(t)\right)dt$$

where m_0 corresponds to the automaticity, and $m_r(t)$ represents the neural input from the arterial baroreflex control system. A new heartbeat occurs when the transmembrane potential $M(t)$ reaches a predefined threshold potential Γ, and the time since the previous heartbeat is at least one fifth of the preceding cardiac cycle length. This last constraint represents the absolute refractory period of the heart cells. Therefore, the heartbeat occurs at t_k when:

$$\int_{t_{k-1}}^{t_k} m(t)dt = M(t_k)\geq\Gamma \quad \text{and}$$

$$t_k-t_{k-1}\geq 0.2\left(t_{k-1}-t_{k-2}\right)$$

The automaticity m_0 is assumed to be constant, which leads to a constant heart rate in the absence of neural input from the sympathetic or parasympathetic control system. Then, the baroreceptor input can either increase (via sympathetic stimulation) or decrease (via parasympathetic stimulation) the slope of the transmembrane potential, increasing or decreasing the generation rate of heartbeats. The function $m(t)$ is defined as the inverse of the instantaneous R–R interval $I(t)$:

$$m(t)=\frac{1}{I(t)}=\frac{1}{I_0+\Delta I_{AB}(t)}$$

where I_0 is the nominal R–R interval, and $\Delta I_{AB}(t)$ represents the control input from the baroreceptor control system. The nominal heart rate is 67 beats/min and the threshold potential Γ is equal to 1.

2.3. Pulmonary circulation

The pulmonary circulation is represented by one arterial compartment and one venous compartment connected in series by the pulmonary microcirculation R_{pv}. The parameters for the pulmonary circulation are shown in Table 6.

2.4. Control systems

The cardiovascular system must assure the delivery of oxygen and nutrients to all parts of the body, as well as the removal of waste. These mechanisms need to be maintained even in the presence of cardiovascular stress such as orthostatic stress due to centrifugation. The arterial baroreflex and the cardiopulmonary reflex are the two major neurally-mediated reflex mechanisms responsible for the short-term hemodynamic response, assuring a proper regulation of the cardiovascular system.

The arterial baroreceptors are stretch receptors located in the aortic arch and carotid sinus, and their main function is to regulate arterial blood pressure. These pressure sensors respond to stretching so that if arterial pressure increases, the arterial wall expands causing an increase in the firing rate of action potentials. Similarly, if pressure suddenly decreases the firing rate of action potentials decreases. These signals travel to the *nucleus tractus solitarious* (NTS), which is located in the medulla of the brainstem, through two sets of nerves: the glossopharyngeal nerves (carotid sinus reflex) and the vagus nerves (aortic arch reflex). Integrating the autonomic responses, the NTS regulates both the sympathetic and parasympathetic activity using efferent pathways to various organs [41].

The cardiopulmonary receptors are located in the atria and the pulmonary arteries. They respond to increases in blood pressure in these low-pressure areas caused by an increase in volume. Thus, when blood volume increases in these areas, the information travels through the vagal afferent nerves to the medulla, leading to a reduction in efferent sympathetic activity [36,38,41]. In addition, the cardiopulmonary reflex is related to the long-term neurohumeral regulation. Stretch of the atria causes an increase of atrial natriuretic peptide (APN), a powerful vasodilator, and a decrease in

Table 6
Pulmonary circulation parameters: C: compliance, V_0: zero-pressure filling volume, R: resistance, and R_{pv}: pulmonary microcirculation.

Parameter	Units	Pulmonary arteries	Pulmonary veins
C	$\frac{\text{ml}}{\text{mmHg}}$	3.4	9.0
V_0	ml	160	430
R	PRU	0.006	0.006
R_{pv}	PRU	0.07	

the secretion of antidiuretic hormone (ADH), causing loss of fluid through urine.

Each reflex mechanism can be represented using a negative feedback loop and a reference pressure [38]. The feedback error signal between the corresponding sensor pressure (either arterial or cardiopulmonary receptors) and the reference pressure is fed to the sympathetic and parasympathetic system (using the appropriate filtering) before constituting the neurally-mediated global reflex contribution to the corresponding effector variables, including heart rate, heart rate contractility, vascular resistance, and venous tone. A schematic of the cardiovascular control system implemented in the model is shown in Fig. 5.

2.4.1. Modeling the arterial baroreflex

The arterial baroreceptor mechanism is represented using a negative feedback loop and an arterial pressure set-point P_A^{sp} as the reference pressure. Only one lumped baroreceptor in the carotid sinus is considered, and it is assumed to be located 25 cm above the location of the heart (represented by the aortic arch pressure P_1). Thus, taking into account the hydrostatic column due to short-radius centrifugation, the carotid sinus pressure P_{CS} (mmHg) is defined as:

$$P_{CS} = P_1 - \frac{1}{2}\cdot\rho\cdot\omega^2(t)\cdot\left((25+d)^2 - d^2\right)$$

where d is the distance between the head and the center of rotation measured in cm, ρ is the blood density in $\frac{\text{mmHg}}{1/s^2\text{cm}^2}$, and $\omega(t)$ is the angular velocity of the centrifuge in rad/s. The feedback error signal $e_{AB}(t)$ is then calculated by subtracting the arterial pressure set-point P_A^{sp} from the carotid sinus pressure P_{CS}, and scaling the resultant signal appropriately [36,38]:

$$e_{AB}(t) = 18\cdot arc\ \tan\left(\frac{P_{CS} - P_A^{sp}}{18}\right)$$

In nominal conditions (no exercise), the value of the arterial pressure set-point P_A^{sp} is 95 mmHg.

The sympathetic and parasympathetic control systems are modeled as two linear time-invariant (LTI) filters, as proposed by Samar [42] and later used by Zamanian [38]. The sympathetic filter is represented using a triangular impulse response function, which is parameterized in terms of three timing variables: a delay, a peak, and an end. The transfer function used for the sympathetic filter is given by:

$$s(s) = \frac{1}{42s^2}e^{-2s} + \frac{1}{75s^2}e^{-5s} + \frac{1}{300s^2}e^{-30s}$$

corresponding to a delay of 2 s, a peak of 5 s, and an end of 30 s (values taken from Samar [42]).

Samar [42] also proposed to represent the parasympathetic transfer function as a simple gain with zero delay. This approximation is valid due to the relatively rapid response of the parasympathetic system and its small time delay of less than one second. Therefore, the parasympathetic filter is given by:

$$p(s) = 1$$

The contribution of the autonomic control system to the effector variables is obtained by convolving the error signal with a linear combination of the sympathetic and parasympathetic control filters. The gains of the filters are specific to each effector variable. The arterial baroreflex contribution is then added to the cardiopulmonary reflex contribution (see following section) to constitute the total neurally-mediated global reflex contribution to each effector variable. The effector variables taken into account in the arterial baroreflex model are heart rate, heart contractility, arterial resistance, and venous unstressed volume [36]. Fig. 6 shows a diagrammatic representation of the arterial baroreflex central nervous processing. The gain values for the arterial baroreflex model are taken from Heldt's model [36] and later used by Zamanian [38]. They are summarized in Table 7.

2.4.2. Modeling the cardiopulmonary reflex

The cardiopulmonary reflex is also represented by a negative feedback loop, using a pressure set-point P_{CP}^{sp} as the reference pressure. The variable measured is the transmural right atrial pressure ΔP_{RA}. The feedback error signal $e_{CP}(t)$ is then calculated by subtracting the set-point pressure P_{CP}^{sp} from the transmural right atrial pressure ΔP_{RA}, and scaling the resultant signal appropriately [36,38]:

$$e_{CP}(t) = 5\cdot arc\ \tan\left(\frac{\Delta P_{RA} - P_{CP}^{sp}}{5}\right)$$

where the reference pressure P_{CP}^{sp} is set to 5 mmHg.

The contribution of the cardiopulmonary reflex to the effector variables is obtained using a similar process to the case of the arterial baroreflex. The cardiopulmonary error signal is fed to the sympathetic and parasympathetic filters previously described, and specific gains are applied to each effector variable. Finally, the cardiopulmonary contribution is added to the arterial baroreflex contribution to constitute the total neurally-mediated global reflex contribution to each effector variable. The effector variables taken into account in the cardiopulmonary reflex model are arterial resistance and venous unstressed volume [36]. The gain values are

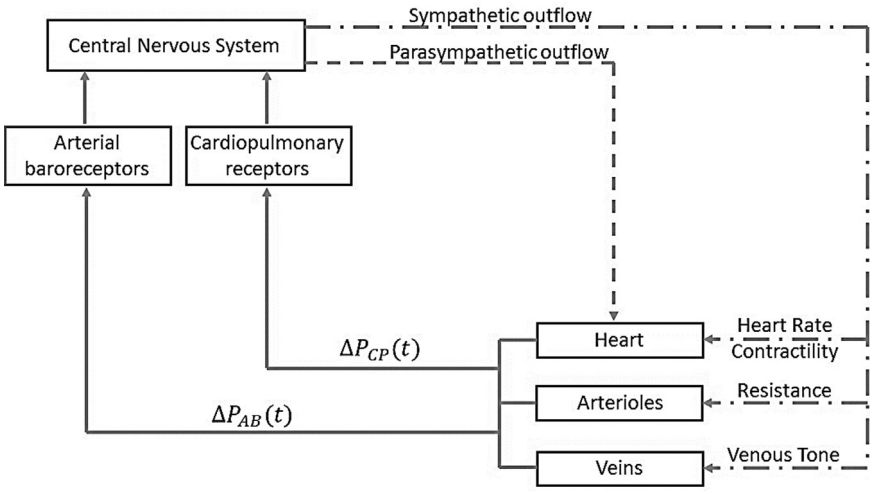

Fig. 5. Cardiovascular control system. $\Delta P_{AB}(t)$, $\Delta P_{CP}(t)$: arterial baroreceptors and cardiopulmonary receptors transmural pressures (figure adapted from [36,38,42]).

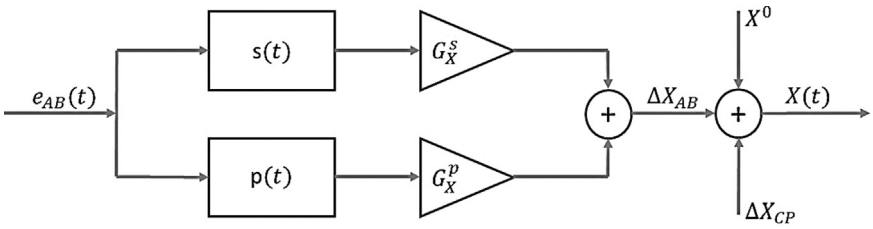

Fig. 6. Arterial baroreflex block diagram of the central nervous processing for an effector variable X. Parameters include $e_{AB}(t)$: feedback error signal; $s(t)$, $p(t)$: sympathetic and parasympathetic control filters; G_X^s, G_X^p: sympathetic and parasympathetic gain values for effector variable X; ΔX_{AB}, ΔX_{CP}: arterial baroreceptor and cardiopulmonary receptor contributions to the effector variable X; X^0: initial value of effector variable X; $X(t)$: current value of effector variable X (adapted from Zamanian [38]).

Table 7
Sympathetic G^s and Parasympathetic G^p gain values for the arterial baroreflex model. Values taken from Heldt [36] and Zamanian [38].

Reflex arc	Units	G^s	G^p
R–R Interval	$\frac{ms}{mm\ Hg}$	9	9
Left ventricular contractility C_{ls}	$\frac{ml}{mm\ Hg^2}$	0.007	0
Right ventricular contractility C_{rs}	$\frac{ml}{mm\ Hg^2}$	0.022	0
Upper body arterial resistance R_{ub}	$\frac{PRU}{mm\ Hg}$	−0.05	0
Renal circulation arterial resistance R_{rc}	$\frac{PRU}{mm\ Hg}$	−0.05	0
Splanchnic circulation arterial resistance R_{sc}	$\frac{PRU}{mm\ Hg}$	−0.05	0
Leg circulation arterial resistance R_{lc}	$\frac{PRU}{mm\ Hg}$	−0.05	0
Upper body venous unstressed volume V_{ub}	$\frac{ml}{mm\ Hg}$	5	0
Renal venous unstressed volume V_{rc}	$\frac{ml}{mm\ Hg}$	2	0
Splanchnic venous unstressed volume V_{sc}	$\frac{ml}{mm\ Hg}$	13	0
Leg venous unstressed volume V_{lc}	$\frac{ml}{mm\ Hg}$	7	0

Table 8
Sympathetic G^s and Parasympathetic G^p gain values for the cardiopulmonary reflex model. Values taken from Heldt [36] and Zamanian [38].

Reflex arc	Units	G^s	G^p
Upper body arterial resistance R_{ub}	$\frac{PRU}{mm\ Hg}$	−0.05	0
Renal circulation arterial resistance R_{rc}	$\frac{PRU}{mm\ Hg}$	−0.05	0
Splanchnic circulation arterial resistance R_{sc}	$\frac{PRU}{mm\ Hg}$	−0.05	0
Leg circulation arterial resistance R_{lc}	$\frac{PRU}{mm\ Hg}$	−0.05	0
Upper body venous unstressed volume V_{ub}	$\frac{ml}{mm\ Hg}$	13	0
Renal venous unstressed volume V_{rc}	$\frac{ml}{mm\ Hg}$	3	0
Splanchnic venous unstressed volume V_{sc}	$\frac{ml}{mm\ Hg}$	64	0
Leg venous unstressed volume V_{lc}	$\frac{ml}{mm\ Hg}$	30	0

taken from Heldt's model [36] and later used by Zamanian [38]. They are summarized in Table 8.

2.5. Modeling centrifugation

The effects of centrifugation are represented by changes in hydrostatic pressure, changes in intra-thoracic pressure, and changes in total blood volume.

The effect of orthostatic stress is primarily represented by pressure sources, P_h, to account for the hydrostatic pressure resulting from centrifugation. These pressure sources are positioned in series within each compartment (see Fig. 7) and their magnitudes depend on the subject positioning on the centrifuge, particularly on the distance between each cardiovascular compartment and the center of rotation of the centrifuge. A mathematical expression for the hydrostatic pressure is given below and in Fig. 7:

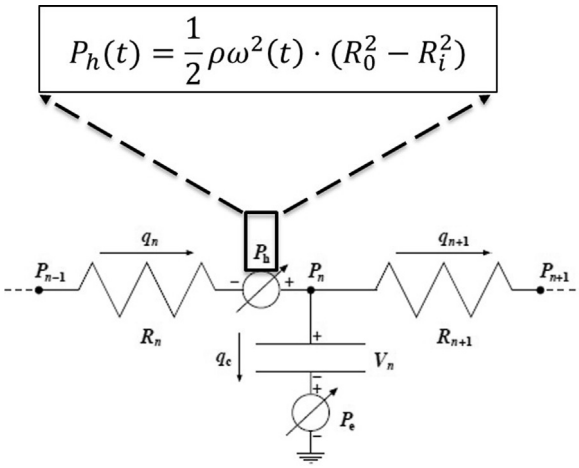

Fig. 7. Pressure sources accounting for the hydrostatic pressure resulting from centrifugation.

$$P_h(t) = \int_{R_i}^{R_o} \rho\cdot\omega^2(t)\cdot dr = \rho\cdot\omega^2(t)\cdot\frac{r^2}{2}\Big|_{R_i}^{R_0} = \frac{1}{2}\rho\omega^2(t)\cdot(R_o^2 - R_i^2)$$

where $\omega(t)$ is the angular velocity of the centrifuge, ρ is the blood density, the inlet radius R_i is the distance between the superior end of the compartment and the center of rotation, and the outlet radius R_o is the sum of the effective height of the compartment and the inlet radius. The effective height is assumed to be one half of the anatomical vertical length for each compartment, except the

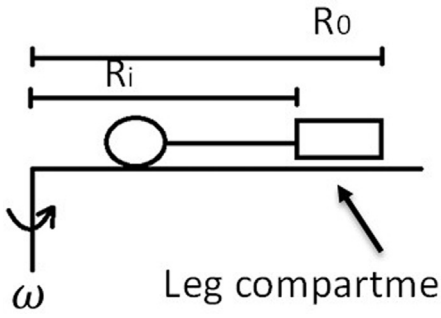

Fig. 8. Example of the subject configuration on the centrifuge and positioning of the leg compartment. The angular velocity ω has been depicted at the center of rotation of the centrifuge. The inlet radius R_i is the distance between the superior end of the compartment and the center of rotation, and the outlet radius R_o is defined as the sum of the effective height of the compartment and the inlet radius.

leg compartments where the effective length is defined as a third of the anatomical vertical length. As an example, Fig. 8 shows a subject lying down on a centrifuge with the feet pointing at the rim of the centrifuge (radially outward direction). The leg compartment is located at a distance R_i from the center of rotation, and its effective height is $h_{lef}=R_o-R_i=\frac{1}{3}l_{v\ legs}$.

Intra-thoracic pressure also changes during orthostatic stress due to the weight of the liver being pulled down in the thoracic compartment [38,43,44]. Based on Heldt's model [36], the intra-thoracic pressure $P_{th}(t)$ during centrifugation is given by:

$$P_{th}(t) = P_{th_0} - 3.5 \cdot \frac{(r+h)^2 \cdot \omega_{max}^2}{g^2} \cdot \omega^2(t)$$

where $r = 55$ cm corresponding to the location of the liver in the thoracic compartment; h is the distance from the head to the center of rotation of the centrifuge in cm; and $\omega(t)$ is the angular velocity. The nominal intra-thoracic pressure P_{th_0} is set to -4 mmHg.

Orthostatic stress causes an increase in transcapillary fluid flow in the dependent vasculature and, as a consequence, a net decrease in intravascular volume. Changes in hydrostatic pressure alter the equilibrium between oncotic and hydrostatic gradients, directly affecting transcapillary fluid exchange. Based on previous studies about transcapillary flow during orthostatic stress, Heldt characterized this phenomenon using additional RC compartments. The transcapillary flow is solved analytically based on the orthostatic stress profile using the equations described in Appendix A. The solution of the equations depend on two parameters: the time constant $\tau = RC$ and the maximum interstitial volume change $V_{max}=P_hC$. For upright tilt and stand test simulations, Heldt proposed a time constant $\tau = 4.6\,min$, value that we maintained for our centrifuge simulations. Lastly, using Heldt and Zamanian's approaches, the maximum interstitial volume change V_{max} during centrifugation is given by:

$$V_{max} = 300\ \text{ml} \cdot \frac{(r+h)\cdot\omega_{max}^2}{g \cdot \sin(85)}$$

where $r = 55$ cm corresponds again to the thoracic compartment; h is the distance from the head to the center of rotation of the centrifuge in cm; and $\omega(t)$ is the angular velocity.

Once the equations are solved, the transcapillary flow is simply subtracted from the venous return at the selected compartments where this phenomenon is significant, namely splanchnic venous (number 11), leg venous (number 13), and abdominal venous (number 14) compartments. The fractions of interstitial volume and interstitial flow assigned to each compartment are defined as follows:

$$V^n(t) = \frac{P_h^n}{\sum_i P_h^i} \cdot V(t)$$

$$q^n(t) = \frac{P_h^n}{\sum_i P_h^i} \cdot q(t)$$

where P_h^n is the hydrostatic pressure in the nth compartment (either 11, 13, or 14); and $\sum_i P_h^i$ is the sum of the hydrostatic pressures of the three compartments (11, 13, and 14).

2.6. Modeling exercise

One of the primary effects of exercise on the cardiovascular system is the large increase in the blood flow to the muscle groups that are exercising [36,41]. During exercise, blood flow through skeletal muscle can increase from 3–4 ml/min per 100 g of muscle (average during rest) to 50–80 ml/min per 100 g of muscle [41]. Three major processes (although all three are interconnected) occur in the circulatory system to supply the increased blood flow required by the muscles: mass sympathetic discharge through the body, increase in arterial pressure, and increase in cardiac output. Other effects of lower-body ergometer exercise include the pump effect of the leg muscles and the increase in intra-abdominal pressure due to the contraction of the abdominal muscles.

In the proposed cardiovascular model, the exercise effects are modeled using four mechanisms: the increase in blood pressure, the increase in blood flow to the exercising muscles due to a decrease in resistance, the action of muscle pumps, and the increase in intra-abdominal pressure. These effects are summarized in Fig. 9.

2.6.1. Increase in arterial blood pressure

In order to capture the effects of increased blood pressure during exercise, an exercise control system is incorporated using a set-point model [36]. The desired exercise workload sets a predefined set-point pressure of the arterial baroreflex P_A^{sp}. Thus, this is an adjustable parameter as a function of exercise intensity. Consequently, the model accounts for changes related to sympathetic activity, namely, increase in heart rate, increase in heart contractility, increase in arterial resistance (except in the active

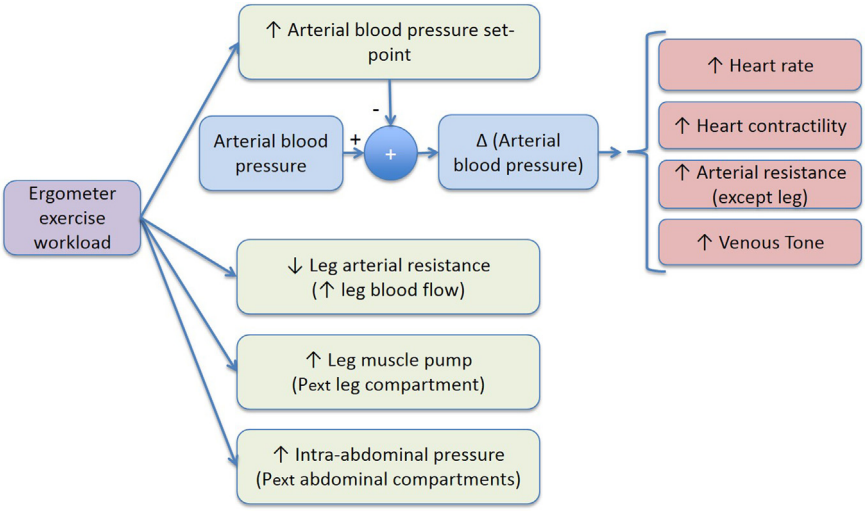

Fig. 9. Exercise effects incorporated in the model.

muscles), and increase in venous tone (decrease in venous zero pressure filling volume).

2.6.2. Decrease in leg arterial resistance

The increase in leg blood flow during ergometer exercise is simulated by disconnecting the leg resistance from the baroreceptor and cardiopulmonary control at the onset of exercise and decreasing it according to:

$$R_{lc}(t)=R_{lc}^{-}+\left(R_{lf}-R_{lc}^{-}\right)(1-e^{-t/\tau})$$

where R_{lc}^{-} is the leg vascular resistance immediately before the onset of an exercise phase, R_{lf} is the final leg vascular resistance for a given exercise intensity, and τ is a time constant. The other three microvascular resistances (upper body R_{ub}, kidneys R_{rc}, and splanchnic R_{sc}) are also disconnected from the baroreflex and cardiopulmonary reflexes and their values are also adjusted to simulate the decrease in total peripheral resistance due to the ergometer exercise. These parameters are chosen manually based on previous experimental data [45,46]. For future simulations, the microvascular resistances remain fully adjustable to simulate different exercise conditions or intensities.

2.6.3. Increase in muscle leg pump

The action of the leg muscle pump during cycling is simulated by varying the external pressure at the venous leg compartment, assuming an ergometer exercise protocol cycling at 1 rev/s. The external pressure is represented according to:

$$P_{ext}^{pump}=\begin{cases} P_{max}^{pump}\frac{1}{2}(1-\cos(4\pi t)) & 0\le t\le 1/4 \\ P_{max}^{pump} & 1/4\le t<1/2 \\ P_{max}^{pump}\frac{1}{2}(1+\cos(4\pi(t-1/2))) & 1/2\le t<3/4 \\ 0 & 3/4\le t<1 \end{cases}$$

where P_{max}^{pump} is the maximal external pressure and it depends on the exercise workload. Fig. 10 depicts an example of the muscle pump modeling, using $P_{max}^{pump}=20$ mmHg.

In addition to the periodic muscle pump effect during cycling, a constant external pressure P_{spin} is also added during the centrifugation periods with no exercise to take into account the activation of the leg muscles when subjects are being pushed against the pedals.

2.6.4. Increase in intra-abdominal pressure

The increase in intra-abdominal pressure is represented by an increase in external pressure on the abdominal compartments (compartments 7, 8, 9, 10, 11, and 14). The external pressure is represented according to:

$$P_{ext}^{abd}=P_{max}^{abd}\,(1-e^{-t/\hat{\tau}})$$

where $\hat{\tau}$ is a time constant and P_{max}^{abd} is the maximal external pressure, which depends on the exercise workload.

2.7. Platform

The cardiovascular model is developed in Matlab Simulink, and it builds upon the previous model developed by Zamanian [38]. In order to avoid problematic numerical errors, the state variable is chosen to be the compartmental distending volume $V_d(t)$. Therefore, the state equation for the compartment n becomes:

$$\frac{d}{dt}V_{dn}(t)=q_{in_n}-q_{out_n}$$

where q_{in_n} and q_{out_n} correspond to the inward and outward compartmental flow respectively.

The model runs using the variable-step solver *ode23t* with a maximum step size of 0.01 s. The initial conditions are calculated using the methodology first implement by David [47], and further developed by Zamanian [38]. The equations are reproduced in Appendix B. This methodology uses a non-linear system of 23 algebraic equations based on first principles to solve for luminal pressures in the compartments and from them, the initial compartmental volumes.

3. Simulation inputs

3.1. Centrifuge configuration

An initial set of simulations was performed to explore the cardiovascular responses to ergometer exercise under different levels of centrifugation, using the MIT CRC as the centrifuge configuration. One of the main characteristics of this centrifuge is that it has been constrained to a radius of 1.4 meters, the upper radial limit for a centrifuge to fit within the Permanent Multipurpose Module (PMM) on-board the International Space Station (ISS). In addition, an ergometer exercise device has been incorporated and therefore, subjects can cycle at the same time as they are being centrifuged. More details of the centrifuge configuration are published elsewhere [48]. Fig. 11 shows the subject positioning on the MIT CRC, which is the configuration that has been taken into account for the simulations. It can be appreciated the bended posture of the subject to be able to fit into a 1.4 m radius centrifuge. The final positioning of the subject on the centrifuge is important, since this ultimately defines the distances between each

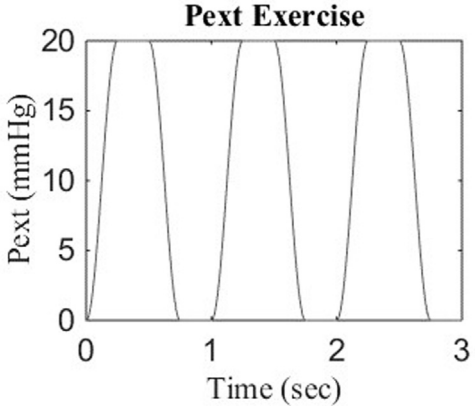

Fig. 10. Example of external pressure due to the muscle pump effect where the maximal external pressure has been set to 20 mmHg. The cycling cadence is 1 rev/s.

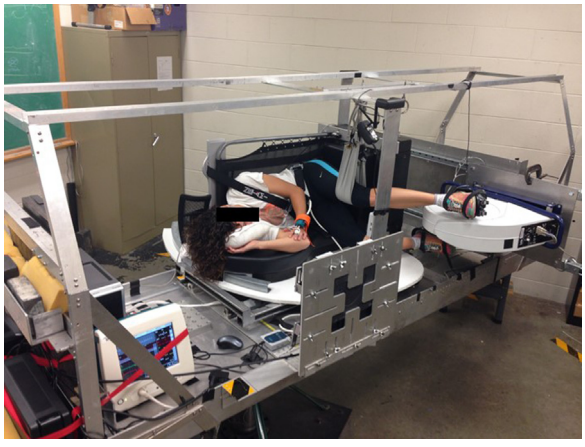

Fig. 11. Subject positioning on the MIT centrifuge. This same configuration was taken into account during the simulations. Figure taken from Diaz [48].

Table 9
Values for inlet radii R_i and outlet radii R_o for all compartments. Subject's head is assumed to be located at the center of rotation ($h = 0$ cm).

Compartment index	R_i (cm)	R_o (cm)
1	24.5	29.5
2	20	22.25
3	0	10
4	0	10
5	20	27.25
6	24.5	32.5
7	40.5	47.75
8	55	55
9	55	55
10	55	60
11	55	60
12	55	83.3
13	55	83.3
14	40.5	47.75
15	34.5	37.5

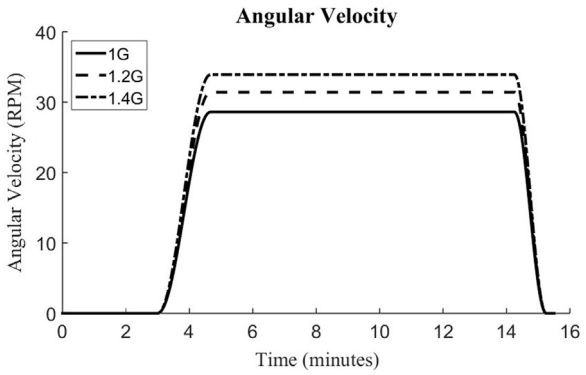

Fig. 12. Angular velocity profile in each one of the three simulations: 1g condition (28.6 RPM), 1.2g condition (31.4 RPM), and 1.4g condition (33.9 RPM). G-levels are referenced to the subject's feet.

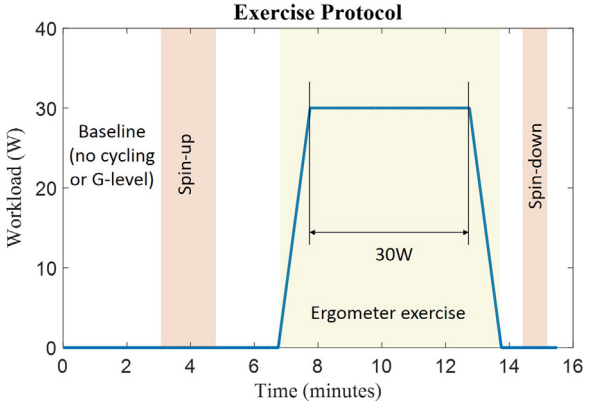

Fig. 13. Exercise protocol.

cardiovascular compartment and the center of rotation of the centrifuge, and therefore, the hydrostatic pressure in each compartment during rotation. Assuming the subject has his/her head at the center of rotation ($h = 0$ cm), the inlet radii R_i and the outlet radii R_o for all compartments are shown in Table 9.

3.2. Artificial gravity and exercise profiles

Three levels of artificial gravity were chosen: 1g, 1.2g, and 1.4g referenced to the subject's feet. These levels correspond to simulated angular velocities of 28.6 RPM (1g condition), 31.4 RPM (1.2g condition), and 33.9 RPM (1.4g condition).

Table 10
Input parameters in the different conditions. The baseline simulation refers to the period where there is no exercise or G-level. The rest of the columns (1g, 1.2g, and 1.4g) show the value of the parameters right after the spin-up process (P_{spin}), or during the exercise period at 30 W (P_A^{sp}, P_{max}^{pump}, P_{max}^{abd}, and resistances R_{lf}, R_{ub}, R_{rc}, R_{sc}).

	Baseline simulation	1g	1.2g	1.4g
P_A^{sp} (mmHg)	95	127	130	134
P_{spin} (mmHg)	0	20	25	30
P_{max}^{pump}(mmHg)	0	54	71	87
P_{max}^{abd} (mmHg)	0	2.5	2.5	2.5
R_{lf} (PRU)	3.9	1	0.95	0.90
R_{ub} (PRU)	3.3	4.5	4.5	4.5
R_{rc} (PRU)	4.1	4.7	4.7	4.7
R_{sc} (PRU)	2.4	3.6	3.6	3.6

Each of the simulations lasted 15.5 min, including a baseline period (3 min with no rotation or exercise), the spin-up process (120 s), the exercise protocol, and the spin-down process (60 s). The exercise protocol consisted primarily of 5 min of ergometer exercise at 30 W of power with a simulated pedal cadence of 60 RPM. Workload transitions were incorporated over 60 s. Fig. 12 depicts the angular velocity profiles in each one of the conditions, and Fig. 13 shows the overall exercise protocol and the specific timeline of the different phases.

3.3. Model parameters

Several parameters were adjusted in each one of the simulated conditions. These parameters include arterial pressure set-point (P_A^{sp}, in mmHg), leg external pressure after spin-up (P_{spin}, in mmHg), maximal leg external pressure during exercise (P_{max}^{pump}, in mmHg), maximal intra-abdominal pressure (P_{max}^{abd}, in mmHg), and the four microvascular resistances: legs R_{lf}, upper body R_{ub}, kidneys R_{rc}, and splanchnic R_{sc}. These values were selected based on previous experimental data and simulations reported elsewhere [45,46]. Table 10 summarizes the input parameters of the cardiovascular simulations in the different conditions, including their baseline value with no exercise or centrifugation. The arterial pressure set-point P_A^{sp} increased slightly according to the centrifugation level to counteract the effects of a higher gravity level. Similarly, the maximal leg external pressure P_{max}^{pump} and the leg external pressure after spin P_{spin}, were slightly larger at faster centrifugation rates due to the higher foot forces generated at higher artificial gravity levels.

As an example, Fig. 14 shows the external pressure exerted by the leg muscles during the simulation at 1 g. The exercise period

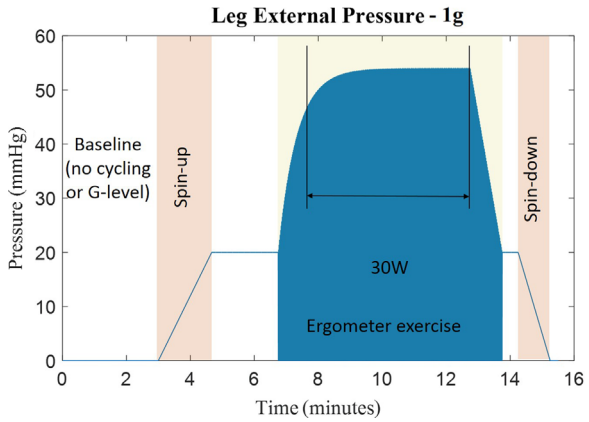

Fig. 14. Leg external pressure due to muscle pump during the 1g simulation.

corresponded to the filled portions of the graph (pressure attained periodically P_{max}^{pump} and 0 mmHg). The workload transition at the beginning of the ergometer exercise was simulated using an exponential function to better capture experimental behavior, using a time constant based on previous experimental data [45,46]. The workload transition at the end of the exercise was represented as a linear function. Furthermore, a constant pressure of P_{spin}=20 mmHg was also added during the centrifugation period with no exercise (after spin-up and before the exercise phase) to simulate the leg muscle activation while subjects are being pushed against the pedals of the cycle ergometer due to the presence of artificial gravity. This pressure P_{spin} was gradually increased during the spin-up phase according to the increase in artificial gravity during this period.

Finally, the total blood volume used in the simulations was V_{tot}=5150 ml. This number was based on the assumption that, in the human body, there are 75 ml of blood per Kg of mass [28,49,50]. Therefore, a total blood volume of 5150 ml corresponds to a subject of approximately 69 Kg. The total zero-pressure filling volume was V_{total}^{0}=4166 ml.

4. Simulation results

Figs. 15 and 16 show the different cardiovascular variables during the simulated 15.5-min exercise protocol at the various levels of centrifugation. Cardiovascular variables include heart rate, mean blood pressure, systolic blood pressure, diastolic blood pressure, stroke volume, cardiac output, vascular resistance, and pulse pressure (defined as the difference between systolic and diastolic blood pressure).

4.1. Spin-up phase

During the spin-up process, the angular velocity of the centrifuge increased from 0 RPM to the desired RPM value using a sinusoidal function (see Fig. 12). The targeted angular velocity was reached over 120 s, corresponding to the shadowed spin-up region on the graphs in Figs. 15 and 16. The simulations are able to capture the spin-up transient cardiovascular responses, which are primarily driven by the increase in hydrostatic pressure that ultimately causes blood pooling towards the lower body. Given the configuration of a short-radius centrifuge and therefore the presence of a strong gravity gradient, the hydrostatic pressure was more important in the compartments located further away from the center of rotation (i.e. lower body). On the other hand, external pressure in the legs increased during the spin-up process due to the small contractions of the leg muscles when pushed against the pedals. This facilitates blood circulation back to the heart and counteracts to some extent the effects of the orthostatic stress caused by centrifugation.

At the beginning of the spin-up process, the vascular resistance, initially at 0.88 PRU (Peripheral Resistance Unit), decreased due to the blood pooling to the lower part of the body. After several seconds, the baroreceptor signal activated the sympathetic stimulation and the vascular resistance slowly increased to 0.91 PRU. The simulated heart rate also responded properly to the orthostatic stress by increasing from 75 bpm to 80 bpm. These cardiovascular regulation actions, prompted by the arterial baroreceptor and cardiopulmonary control systems, were able to keep the mean blood pressure relatively constant around 88 mmHg. Stroke volume decreased from 76 ml to ~70 ml, but cardiac output remained fairly constant at ~5.8 l/min, presumably due to the increase in venous return caused by the leg external pressure. Finally, pulse pressure decreased from 42 mmHg to ~38 mmHg due

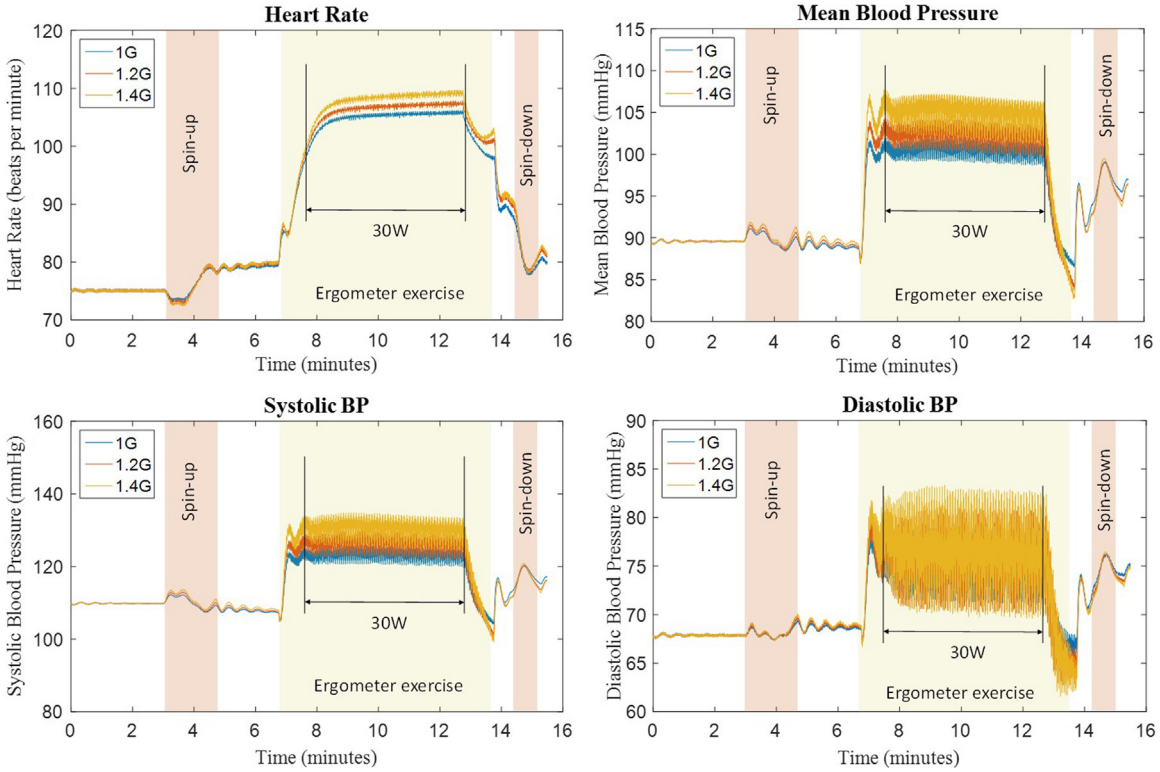

Fig. 15. Cardiovascular variables (Heart Rate, Mean Blood Pressure, Systolic Blood Pressure, and Diastolic Blood Pressure) simulated during the 15.5-min exercise protocol at each one of the three artificial gravity conditions: 1*g* (blue line), 1.2*g* (orange line), and 1.4*g* (yellow line). Gravity levels are simulated at the subject's feet (subject's head is assumed to be located at the center of rotation of the centrifuge). (For interpretation of the references to color in this figure legend, the reader is referred to the web version of this article.)

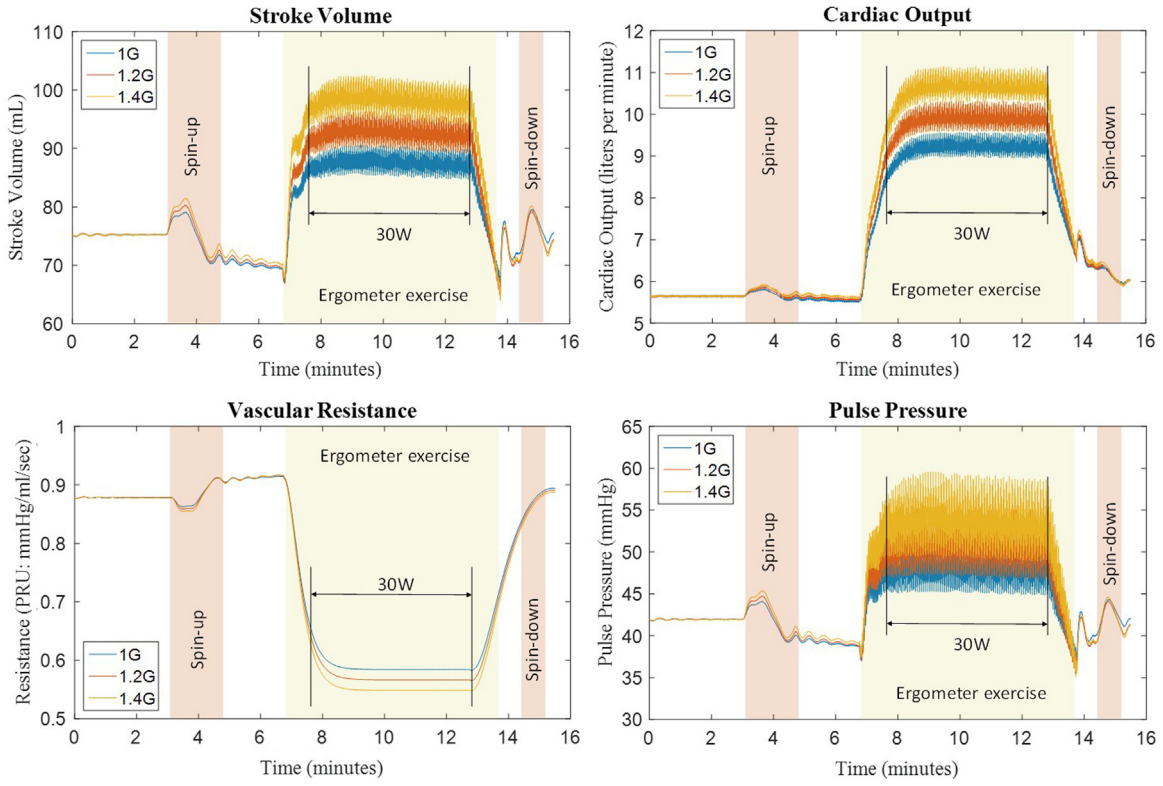

Fig. 16. Cardiovascular variables (Stroke Volume, Cardiac Output, Vascular Resistance, and Pulse Pressure) simulated during the 15.5-min exercise protocol at each one of the three artificial gravity conditions: 1*g* (blue line), 1.2*g* (orange line), and 1.4*g* (yellow line). Gravity levels are simulated at the subject's feet (subject's head is assumed to be located at the center of rotation of the centrifuge). (For interpretation of the references to color in this figure legend, the reader is referred to the web version of this article.)

to slight decrease in systolic blood pressure and a slight increase in diastolic blood pressure.

During the spin-up period and before the exercise phase, differences between the three gravity levels were not very substantial, although they were still noticeable.

In general, transient responses during the spin-up process at higher g-levels were slightly more prominent, particularly stroke volume, pulse pressure, and vascular resistance. However, after the spin-up transient period (i.e. once the angular velocity reached its final, constant value), the cardiovascular variables presented very similar responses across gravity levels, despite the stronger blood pooling effect created at higher g-levels.

4.2. Exercise phase

The simulation of ergometer exercise activity caused a significant change in the operating point of all the cardiovascular variables. The vascular resistance decreased considerably to allow higher blood flow to reach the exercising muscles, and satisfy their higher energetic demand. As mentioned in previous paragraphs, the vascular resistance was disconnected from the control systems at the onset of the exercise and was manually decreased to the values shown in Table 10, according the g-level (higher g-levels were associated to a lower vascular resistance to account for the more intense exercise caused by the higher centrifugal acceleration). Thus, vascular resistance can be considered an input to the simulation. As expected, heart rate, blood pressure, stroke volume, and cardiac output increased during exercise.

Differences across g-levels are very noticeable in most of the cardiovascular variables. Heart rate increased slightly with g-level, presumably to respond to the stronger blood pooling towards the lower body. Interestingly, mean blood pressure also increased with g-level. This behavior could be explained by the fact that at higher g-level, despite the stronger blood pooling to the lower extremities, the venous return was facilitated and maintained by the higher foot forces exerted on the cycle ergometer during exercise. Therefore, this exercise effect, combined with the higher sympathetic activity, caused the systolic blood pressure to slightly increase. On the other hand, minimum values of diastolic blood pressure decreased in the presence of centrifugation pooling blood to the lower body. As a result, pulse pressure also increased with artificial gravity level during ergometer exercise. Stroke volume and cardiac output also increased according to the g-level.

4.3. Post-exercise and spin-down phase

The exercise period finalized after 60 seconds of ramp-down, where the workload intensity was decreased from 30 W to 0 W. During this time, all cardiovascular variables initiated their return to their original values before the exercise period. In general, the cardiovascular behavior during the spin-down process was the opposite to the spin-up process (see stroke volume, pulse pressure, heart rate, and blood pressure). Vascular resistance was again manually increased to its initial value using a sinusoidal function. This resistance was kept disconnected from the control systems and therefore, it is still considered an input to the model. In this scenario, the vascular resistance remained independent of the spin-down process and therefore, the cardiovascular results in this region must be interpreted with caution.

5. Discussion

Artificial gravity has been suggested as a multi-system countermeasure against the debilitating effects of extended weightlessness. The different approaches to development and validation have served as the emphasis of at least three major international working groups over the past 15 years [51–53]. Among the

numerous critical design questions remain those of centrifuge radius, g-level, gravity gradient, or exercise. Mathematical simulations are certainly an affordable approach to understand the physiological responses in altered-gravity environment, and the important trade-offs between the multiple parameters and possible configurations.

The cardiovascular model developed here is able to make quantitative predictions on several cardiovascular variables (including blood pressure, heart rate, stroke volume, and cardiac output) during ergometer exercise in altered-gravity generated using a short-radius centrifuge. The model is composed of 21 compartments representing different parts of the cardiovascular system, namely the systemic circulation, cardiac chambers, and the pulmonary circulation. The high number of compartments, particularly in the Gx axis, allows for changes in hydrostatic pressure along the body that account for the presence of a strong gravity gradient when spinning in a short radius centrifuge. In addition, the model also incorporates the two major neurally-mediated control mechanisms: the arterial baroreflex and the cardiopulmonary reflex. Furthermore, the effects of ergometer exercise were also incorporated in the model, including the increase in blood pressure, the muscle pump effect, the decrease in vascular resistance, and the slight increase in intra-abdominal pressure. This model builds on previous contributions from Heldt [36] and Zamanian [38] and, to our knowledge, this is the first cardiovascular model that has the ability to incorporate exercise in the presence of gravity-gradient environments. Due to the MIT experimental set-up (see Fig. 11), we chose to simulate lower body cycling exercise, but other types of exercise (e.g. squats or upper body exercise) could be easily incorporated following a similar approach.

The model integrates different inputs to define the operating point of the desired simulation. Inputs include centrifuge configuration (i.e. centrifuge length), the subject positioning on the centrifuge (i.e. distance from the head and other compartments to the center of rotation), the centrifugation angular velocity, and exercise protocol. In this particular case, we performed a set of simulations representing an ergometer exercise protocol in the new configuration of the MIT centrifuge [48]. Three equally-shaped artificial gravity profiles were simulated, attaining different angular velocities: 28.6 RPM, 31.4 RPM, and 33.9 RPM, generating 1*g*, 1.2*g*, and 1.4*g* of artificial gravity referenced to the subject's feet respectively. The simulated protocol included a baseline period, a spin-up phase, an exercise phase (simulating an ergometer workload of 30 W), and a spin-down-phase.

All cardiovascular variables responded appropriately to the orthostatic stress induced by the spin-up process. Variable transients during the acceleration profile were well captured and the amplitude of these changes increased with the g-level. These results indicate the ability of the cardiovascular control systems, combined with the benefits of small leg muscle contractions, to regulate properly at the simulated levels of artificial gravity. After the spin-up phase and once the angular velocity was stable, differences between g-levels were not as noticeable. This could be explained by the positioning of the subject and the presence of the strong gravity gradient associated with such as short-radius centrifuge. Thus, even if the artificial gravity levels generated at the feet are considerably different, those differences get smaller in the upper body and ultimately disappear at the head, which is located at the center of rotation and therefore the centripetal acceleration is zero in all conditions. Additionally, the simulations also captured the cardiovascular changes that occurred during the exercise period. Heart rate, stroke volume, and cardiac output increased to satisfy the new metabolic demand imposed by the exercise activity. In addition, simulations indicated that, during exercise, stroke volume, cardiac output, pulse pressure, and to a lesser extent, heart rate increased with g-level. These results suggest that, despite the stronger blood pooling effect, ergometer exercise at higher g-levels increased venous return, facilitated by the stronger muscle pump effect presumably due to higher foot forces.

The lumped-parameter nature of the model entails some limitations. First, these types of models provide beat-to-beat averaged cardiovascular values, which significantly reduces the computational cost. Given our particular application, the use of a lumped-parameter model is a reasonable choice, but this is not appropriate for other applications interested in more detailed hemodynamic data within the cardiac cycle. Additionally, these models do not capture appropriately hemodynamic changes along the body such as wave transmission phenomena or hemodynamic distal changes [39,54].

The lumped-parameter model developed in this research effort provides a unique insight into the cardiovascular regulation under artificial gravity combined with exercise. The large number of cardiovascular compartments, particularly in the longitudinal axis of the body, makes this model an excellent approach to capture the effects of the strong gravity gradient generated in a short-radius centrifuge. This paper provides a deep technical description of the different cardiovascular elements incorporated in the model, including previous work from Heldt [36] and Zamanian [38], with the objective of making it fully reproducible by the reader. In addition, the initial simulations presented here provide a first look into the capabilities of the model, which is able to capture both the cardiovascular dynamics during gravity changes, and steady-state responses during sustained artificial gravity levels and exercise. The model has also been further evaluated and validated using experimental data from the combined exercise and artificial gravity experiments conducted on the MIT CRC, and these results will be presented separately in future publications. This cardiovascular model can simulate a variety of centrifuge configurations and exercise intensities without the need of performing additional human experiments. Future simulations should include different centrifuge configurations and exercise protocols, exploring both hyper-gravity (greater than 1*g*) and hypo-gravity (between 0–1*g*) altered-gravity levels.

Acknowledgment

This project was supported by the MIT/Skolkovo Development Project (Seed Grant 6925991), and the National Space Biomedical Research Institute through NASA NCC 9-58. In addition, the Fulbright Commission has provided additional support.

Appendix A

The following equations, taken from Heldt [36], provide an analytical solution for the intercapillary flow and interstitial volume change during gravitational stress. The solution has been divided in four regions, depending on the nature of the orthostatic stress. The regions are indicated in Fig. 17.

Region I: Gradual increase in orthostatic stress over a period of length Δt.

$$q(t)=\frac{V_{max}}{\Delta t}\cdot(1-e^{-\frac{t}{\tau}}) \tag{A1}$$

$$V(t)=V_{max}\cdot\left(\frac{t}{\Delta t}-\frac{\tau}{\Delta t}\left(1-e^{-\frac{t}{\tau}}\right)\right) \tag{A2}$$

Region II: Full orthostatic stress during period of duration T_{tilt}.

$$q(t)=\frac{V_{max}}{\Delta t}\cdot\left(1-e^{-\frac{\Delta t}{\tau}}\right)\cdot e^{-\frac{t-\Delta t}{\tau}} \tag{A3}$$

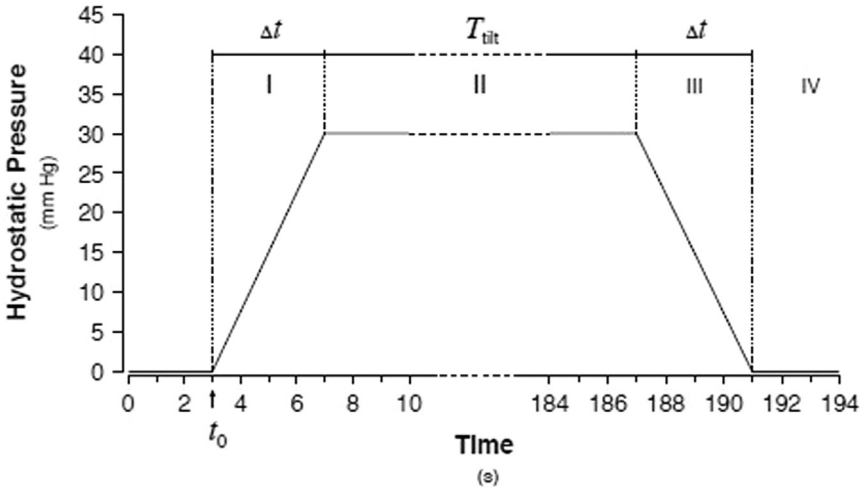

Fig. 17. Generic hydrostatic pressure profile. Figure taken from [36].

$$V(t)=V_{max}\cdot\left(1-\frac{\tau}{\Delta t}\left(1-e^{-\frac{\Delta t}{\tau}}\right)e^{-\frac{t-\Delta t}{\tau}}\right) \tag{A4}$$

Region III: Gradual decline in orthostatic stress over a period of length Δt.

$$q(t)=\frac{V_{max}}{\Delta t}\cdot\left(1+\left(1-e^{-\frac{\Delta t}{\tau}}\right)e^{-\frac{T_{tilt}}{\tau}}\right)\cdot e^{-\frac{t-(\Delta t+T_{tilt})}{\tau}}-\frac{V_{max}}{\Delta t} \tag{A5}$$

$$V(t)=V_{max}\cdot\left(1-\frac{t-(\Delta t+T_{tilt})}{\Delta t}\right)-V_{max}\cdot\frac{\tau}{\Delta t}\cdot\left(1-e^{-\frac{\Delta t}{\tau}}\right)\cdot e^{-\frac{T_{tilt}}{\tau}}+V_{max}\cdot\frac{\tau}{\Delta t}\cdot\left(1+\left(1-e^{-\frac{\Delta t}{\tau}}\right)e^{-\frac{T_{tilt}}{\tau}}\right)\cdot\left(1-e^{-\frac{t-(\Delta t+T_{tilt})}{\Delta t}}\right) \tag{A6}$$

Region IV: Post-orthostatic stress recovery of unspecified length.

$$q(t)=-\frac{V_{max}}{\Delta t}\cdot\left(1-e^{-\frac{\Delta t}{\tau}}\right)\cdot\left(1-e^{-\frac{T_{tilt}+\Delta t}{\tau}}\right)\cdot e^{-\frac{t-(2\Delta t+T_{tilt})}{\tau}} \tag{A.7}$$

$$V(t)=V_{max}\cdot\frac{\tau}{\Delta t}\cdot\left(1-e^{-\frac{\Delta t}{\tau}}\right)\cdot\left(1-e^{-\frac{T_{tilt}+\Delta t}{\tau}}\right)\cdot e^{-\frac{t-(2\Delta t+T_{tilt})}{\tau}} \tag{A.8}$$

Appendix B

The 23 non-linear algebraic equations to find the initial conditions used by Zamanian [38] are listed below. The first equation equates the right ventricular stroke volume and the left ventricular stroke volume. The following 21 equations describe the blood flow in the compartments assuming that the capacitors are not conducting. The last equation is based on the conservation of volume equating the difference between the total volume and the unstressed volume, and the distending volume in each compartment.

$$C_{ld}(P_{lvd}-P_{th})-C_{ls}(P_{lvs}-P_{th})=C_{rd}(P_{rvd}-P_{th})-C_{rs}(P_{rvs}-P_{th}) \tag{B1}$$

$$C_{ld}(P_{lvd}-P_{th})-C_{ls}(P_{lvs}-P_{th})=T_s^v\cdot\frac{P_{lvd}}{R_1} \tag{B2}$$

$$T_s^v\cdot\frac{P_{lvd}}{R_1}=I_0\cdot\left(\frac{P_1-P_2}{R_2}+\frac{P_1-P_6}{R_6}\right) \tag{B3}$$

$$I_0\cdot\frac{P_1-P_2}{R_2}=I_0\cdot\frac{P_2-P_3}{R_3} \tag{B4}$$

$$I_0\cdot\frac{P_2-P_3}{R_3}=I_0\cdot\frac{P_3-P_4}{R_{ub}} \tag{B5}$$

$$I_0\cdot\frac{P_3-P_4}{R_{ub}}=I_0\cdot\frac{P_4-P_5}{R_4} \tag{B6}$$

$$I_0\cdot\frac{P_4-P_5}{R_4}=I_0\cdot\frac{P_5-P_{ra}}{R_5} \tag{B7}$$

$$I_0\cdot\frac{P_1-P_6}{R_6}=I_0\cdot\frac{P_6-P_7}{R_7} \tag{B8}$$

$$I_0\cdot\frac{P_6-P_7}{R_7}=I_0\cdot\left(\frac{P_7-P_8}{R_8}+\frac{P_7-P_{10}}{R_{10}}+\frac{P_7-P_{12}}{R_{12}}\right) \tag{B9}$$

$$I_0\cdot\frac{P_7-P_8}{R_8}=I_0\cdot\frac{P_8-P_9}{R_{rc}} \tag{B10}$$

$$I_0\cdot\frac{P_8-P_9}{R_{rc}}=I_0\cdot\frac{P_9-P_{14}}{R_9} \tag{B11}$$

$$I_0\cdot\frac{P_7-P_{10}}{R_{10}}=I_0\cdot\frac{P_{10}-P_{11}}{R_{sc}} \tag{B12}$$

$$I_0\cdot\frac{P_{10}-P_{11}}{R_{sc}}=I_0\cdot\frac{P_{11}-P_{14}}{R_{11}} \tag{B13}$$

$$I_0\cdot\frac{P_7-P_{12}}{R_{12}}=I_0\cdot\frac{P_{12}-P_{13}}{R_{lc}} \tag{B14}$$

$$I_0 \cdot \frac{P_{12}-P_{13}}{R_{lc}} = I_0 \cdot \frac{P_{13}-P_{14}}{R_{13}} \tag{B15}$$

$$I_0 \cdot \frac{P_{14}-P_{15}}{R_{14}} = I_0 \cdot \left(\frac{P_9-P_{14}}{R_9} + \frac{P_{11}-P_{14}}{R_{11}} + \frac{P_{13}-P_{14}}{R_{13}} \right) \tag{B16}$$

$$I_0 \cdot \frac{P_{14}-P_{15}}{R_{14}} = I_0 \cdot \frac{P_{15}-P_{ra}}{R_{15}} \tag{B17}$$

$$I_0 \cdot \left(\frac{P_5-P_{ra}}{R_5} + \frac{P_{15}-P_{ra}}{R_{15}} \right) = T_d^v \cdot \frac{P_{ra}-P_{rvd}}{R_{tri}} \tag{B18}$$

$$T_d^v \cdot \frac{P_{ra}-P_{rvd}}{R_{tri}} = T_s^v \cdot \frac{P_{rvd}-P_{pa}}{R_{ro}} \tag{B19}$$

$$T_s^v \cdot \frac{P_{rvd}-P_{pa}}{R_{ro}} = I_0 \cdot \frac{P_{pa}-P_{pv}}{R_{pv}} \tag{B20}$$

$$I_0 \cdot \frac{P_{pa}-P_{pv}}{R_{pv}} = I_0 \cdot \frac{P_{pv}-P_{la}}{R_{li}} \tag{B21}$$

$$I_0 \cdot \frac{P_{pv}-P_{la}}{R_{li}} = T_d^v \cdot \frac{P_{la}-P_{lvd}}{R_{mit}} \tag{B22}$$

$$V_{total}-V_{total}^0 = \sum_{j \in \left\{ \begin{matrix} 1,2,\ldots,10, \\ 12,15,ra,rv, \\ pa,pv,la,lv \end{matrix} \right\}} C_j \cdot \Delta P_j + \sum_{k \in \{11,13,14\}} \left[\frac{2V_{maxk}}{\pi} \cdot arc\tan\left(\frac{\pi C_{0k}}{2V_{maxk}} \cdot \Delta P_k \right) \right] \tag{B23}$$

where:

C_{ld}: left ventricular diastolic compliance
C_{ls}: left ventricular systolic compliance
C_{rd}: right ventricular diastolic compliance
C_{rs}: right ventricular systolic compliance
P_{lvd}: left ventricular diastolic pressure
P_{lvs}: left ventricular systolic pressure
P_{rvd}: right ventricular diastolic pressure
P_{rvs}: right ventricular systolic pressure
P_{th}: intra-thoracic pressure
T_s^v: ventricular systolic interval
T_d^v: ventricular diastolic interval
I_0: inter-beat interval
P_n: pressure compartment n
R_n: resistance compartment n
R_{ub}: upper body microvascular resistance
R_{rc}: renal microvascular resistance
R_{sc}: splanchnic microvascular resistance
R_{lc}: lower body microvascular resistance
R_{tri}: tricuspid valve resistance
R_{ro}: right ventricular outflow resistance
R_{pv}: pulmonary microcirculation resistance
R_{li}: pulmonary venous outflow resistance
R_{mit}: mitral valve resistance
P_{ra}: right atrial pressure
P_{pa}: pulmonary arterial pressure
P_{pv}: pulmonary venous pressure
P_{la}: left atrial pressure
V_{total}: total blood volume
V_{total}^0: total zero-pressure filling volume
V_{max}: maximal distending volume in venous compartments 11, 13, and 14

References

[1] A.R. Hargens, S. Richardson, Cardiovascular adaptations, fluid shifts, and countermeasures related to space flight, Respir. Physiol. Neurobiol. 169 (SUPPL) (2009) S30–S33.
[2] A.I. Grigoriev, A.R. Kotovskaya, G.A. Fomina, The human cardiovascular system during space flight, Acta Astronaut. 68 (9–10) (2011) 1495–1500.
[3] R.L. Hughson, J.K. Shoemaker, A.P. Blaber, P. Arbeille, D.K. Greaves, P.P. Pereira-Junior, D. Xu, Cardiovascular regulation during long-duration spaceflights to the International Space Station, J. Appl. Physiol. 112 (5) (2012) 719–727.
[4] P. Norsk, Blood pressure regulation IV: adaptive responses to weightlessness, Eur. J. Appl. Physiol. 114 (3) (2014) 481–497.
[5] P. Norsk, A. Asmar, M. Damgaard, N.J. Christensen, Fluid shifts, vasodilatation and ambulatory blood pressure reduction during long duration spaceflight, J. Physiol. 593 (3) (2015) 573–584.
[6] J.C. Buckey, Space Physiology, Oxford University Press, New York, 2006.
[7] G. Clément, A.P. Bukley, Artificial Gravity, Springer, Hawthorne, CA, 2007.
[8] J.C. Buckey, L.D. Lane, B.D. Levine, D.E. Watenpaugh, S.J. Wright, W.E. Moore, F. A. Gaffney, C.G. Blomqvist, Orthostatic intolerance after spaceflight, J. Appl. Physiol. 81 (1996) 7–18.
[9] I.B. Kozlovskaya, A.I. Grigoriev, Russian system of countermeasures on board of the International Space Station (ISS): the first results, Acta Astronaut. 55 (2004) 233–237.
[10] G. Clément, A. Pavy-Le Traon, Centrifugation as a countermeasure during actual and simulated microgravity: a review, Eur. J. Appl. Physiol. 92 (3) (2004) 235–248.
[11] S. Trappe, D. Costill, P. Gallagher, A. Creer, J.R. Peters, H. Evans, Da Riley, R. H. Fitts, Exercise in space: human skeletal muscle after 6 months aboard the International Space Station, J. Appl. Physiol. 106 (2009) 1159–1168.
[12] J.L. Edmonds, T. Jarchow, L.R. Young, Physiological benefits of exercise in artificial gravity: A broadband countermeasure to space flight related deconditioning, Acta Astronaut. 63 (1–4) (2008) 2–7.
[13] H. Akima, K. Katayama, K. Sato, Intensive cycle training with artificial gravity maintains muscle size during bed rest, Aviat Space Environ Med. 76 (2005) 923–929.
[14] E.G. Caiani, P. Massabuau, L. Weinert, P. Vaida, R.M. Lang, Effects of 5 days of head-down bed rest, with and without short-arm centrifugation as countermeasure, on cardiac function in males (BR-AG1 study), J. Appl. Physiol. 117 (6) (2014) 624–632.
[15] K.I. Iwasaki, R. Zhang, J.H. Zuckerman, Ja Pawelczyk, B.D. Levine, Effect of head-down-tilt bed rest and hypovolemia on dynamic regulation of heart rate and blood pressure, Am. J. 279 (6) (2000) R2189–R2199.
[16] D. Linnarsson, R.L. Hughson, K.S. Fraser, G. Clément, L.L. Karlsson, E. Mulder, W.H. Paloski, J. Rittweger, F.L. Wuyts, J. Zange, Effects of an artificial gravity countermeasure on orthostatic tolerance, blood volumes and aerobic power after short-term bed rest (BR-AG1), J. Appl. Physiol. 118 (1) (2015) 29–35.
[17] T. Trappe, S. Trappe, G. Lee, J. Widrick, R. Fitts, D. Costill, Cardiorespiratory responses to physical work during and following 17 days of bed rest and spaceflight, J. Appl. Physiol. 100 (3) (2006) 951–957.
[18] Y.C. Wang, C. Bin Yang, Y.H. Wu, Y. Gao, D.Y. Lu, F. Shi, X.M. Wei, X.Q. Sun, Artificial gravity with ergometric exercise as a countermeasure against cardiovascular deconditioning during 4 days of head-down bed rest in humans, Eur. J. Appl. Physiol. 111 (9) (2011) 2315–2325.
[19] V.A. Convertino, D.F. Doerr, D.L. Eckberg, J.M. Fritsch, J. Vernikos-Danellis, Head-down bed rest impairs vagal baroreflex responses and provokes orthostatic hypotension, J. Appl. Physiol. 68 (1990) 1458–1464.
[20] A.C. Guyton, T.G. Coleman, H.J. Granger, Circulation: overall regulation, Annu. Rev. Physiol. 34 (1972) 13–46.
[21] A.C. Guyton, C.E. Jones, T.G. Coleman, Circulatory Physiology: Cardiac Output and Its Regulation, 2nd ed., WB Saunders, Philadelphia, 1973.
[22] A.C. Guyton, A.E. Taylor, H.J. Granger, Circulatory Physiology II: Dynamics and Control of the Body Fluids, 1st ed., WB Saunders, Philadelphia, 1975.
[23] B.N. Van Vliet, J. Montani, Circulation and Fluid Volume Control, Integr. Physiol. C (2005) 43–66.
[24] J. Montani, B.N. Van Vliet, Understanding the contribution of Guyton's large circulatory model to long-term control of arterial pressure, Exp. Physiol. 94 (2009) 381–397.

[25] L. Taelman, J. Degroote, P. Verdonck, J. Vierendeels, P. Segers, Modeling hemodynamics in vascular networks using a geometrical multiscale approach: numerical aspects, Ann. Biomed. Eng. 41 (7) (2013) 1445–1458.
[26] F.M. Melchior, R.S. Srinivasan, J.B. Charles, Mathematical modeling of human cardiovascular system for simulation of orthostatic response, Am. J. Physiol. 262 (102) (1992) H1920–H1933.
[27] M.S. Olufsen, J.T. Ottesen, H.T. Tran, L.M. Ellwein, La Lipsitz, V. Novak, Blood pressure and blood flow variation during postural change from sitting to standing: model development and validation, J. Appl. Physiol. 99 (2005) 1523–1537.
[28] T. Heldt, E.B. Shim, R.D. Kamm, R.G. Mark, Computational modeling of cardiovascular response to orthostatic stress, J. Appl. Physiol. 92 (2002) 1239–1254.
[29] K. van Heusden, J. Gisolf, W.J. Stok, S. Dijkstra, J.M. Karemaker, Mathematical modeling of gravitational effects on the circulation: importance of the time course of venous pooling and blood volume changes in the lungs, Am. J. 291 (2006) H2152–H2165.
[30] E. Lim, G.S.H. Chan, S. Dokos, S.C. Ng, La Latif, S. Vandenberghe, M. Karunanithi, N.H. Lovell, A cardiovascular mathematical model of graded head-up tilt, PLoS One 8 (2013) e77357.
[31] R.C. Croston, J. a Rummel, F.J. Kay, Computer model of cardiovascular control system responses to exercise, J. Dyn. Syst. Meas. Control 95 (1973) 301–307.
[32] F.M. Melchior, R.S. Srinivasan, P.H. Thullier, J.M. Clère, Simulation of cardiovascular response to lower body negative pressure from 0 to −40 mmHg, J. Appl. Physiol. 77 (1994) 630–640.
[33] R.J. White, J.I. Leonard, J.B. Charles, Mathematical modeling of acute and chronic cardiovascular changes during extended duration orbiter (EDO) flights, Acta Astronaut. 23 (1991) 41–51.
[34] R.J. White, C.G. Blomqvist, Central venous pressure and cardiac function during spaceflight, J. Appl. Physiol. 85 (2) (1998) 738–746.
[35] W.D. Lakin, S.A. Stevens, P.L. Penar, Modeling intracranial pressures in microgravity: the influence of the blood-brain barrier, Aviat. Space Environ. Med. 78 (10) (2007) 932–936.
[36] T. Heldt, Computational Models of Cardiovascular Response to Orthostatic Stress (Ph.D thesis), Massachusetts Institute of Technology, Cambridge, MA, 2004.
[37] T. Heldt, R. Mukkamala, G.B. Moody, R.G. Mark, CVSim: an open-source cardiovascular simulator for teaching and research, Open Pacing Electrophysiol. Ther. J. 3 (2010) 45–54.
[38] S.A. Zamanian, Modeling and Simulating Human Cardiovascular Response to Acceleration (MS thesis), Massachusetts Institute of Technology, Cambridge, MA 02139 41: Philadelphia, PA 19106, 2007.
[39] N. Westerhof, J.W. Lankhaar, B.E. Westerhof, The arterial windkessel, Med. Biol. Eng. Comput. 47 (2009) 131–141.
[40] R.W. de Boer, J.M. Karemaker, J. Stracke, Description of the heart_rate variability data in accordance with a physiological model for the genesis of heartbeats, Phychophysiology 22 (2) (1985) 147–155.
[41] A.C. Guyton, Textbook of Medical Physiology, 8th ed., Harcourt College Pub, 1990.
[42] Z. Samar, Cardiovascular Parameter Estimation using a Computational Model (MS thesis), Massachusetts Institute of Technology, Cambridge, MA 02139 41: Philadelphia, PA 19106, 2005.
[43] J. Mead, E.A. Geansler, Esophageal and pleural pressures in man, upright and supine, J. Appl. Physiol. 14 (1) (1959) 81–83.
[44] B.G. Ferris, J. Mead, N.R. Frank, Effect of body position on esophageal pressure and measurement of pulmonary compliance, J. Appl. Physiol. 14 (4) (1959) 521–524.
[45] A. Diaz Artiles, Exercise under Artificial Gravity – Experimental and Computational Approaches (Ph.D. thesis), Massachusetts Institute of Technology, Cambridge, MA 02139 41: Philadelphia, PA 19106, 2015.
[46] A. Diaz, T. Heldt, L.R. Young, Cardiovascular responses to artificial gravity combined with exercise. in: 2015 IEEE Aerospace Conference Proceedings, Big Sky, MT, 2015.
[47] T. David, Teaching Physiology Through Interactive Simulation of Hemodynamics (MS Thesis), Massachusetts Institute of Technology, Cambridge, MA 02139 41: Philadelphia, PA 19106, 1991.
[48] A. Diaz, C. Trigg, L.R. Young, Combining ergometer exercise and artificial gravity in a compact-radius centrifuge, Acta Astronaut. 113 (2015) 80–88.
[49] B.Y.J.G. Gibson, W.A. Evans, Clinical studies of the blood volume. II. The relation of plasma and total blood volume to venous pressure, blood velocity rate, physical measurements, age and sex in ninety normal humans, J. Clin. Invest. 16 (3) (1937) 317–328.
[50] T. Sjöstrand, Volume and distribution of blood and their significance in regulating the circulation, Physiol. Rev. 33 (2) (1953) 202–228.
[51] W.H. Paloski, L.R. Young, Artificial Gravity Workshop, Proceedings & Recommendations. NASA & NSBRI, League City, Texas, January 14–15, 1999.
[52] L.R. Young, K. Yajima, W.H. Paloski, Artificial Gravity Research to Enable Human Space Exploration, International Academy of Astronautics (IAA), 2009.
[53] W.H. Paloski, J.B. Charles, 2014 International Workshop on Research and Operational Considerations for Artificial Gravity Countermeasures, NASA Ames Research Center, February 19–20, 2014.
[54] I. Kokalari, T. Karaja, M. Guerrisi, Review on lumped parameter method for modeling the blood flow in systemic arteries, J. Biomed. Sci. Eng. 6 (2013) 92–99.